A Comparison of De-noising Methods for Differential Phase Shift and Associated Rainfall Estimation

HU Zhiqun[1,2*] (胡志群), LIU Liping[1] (刘黎平), WU Linlin[3] (吴林林), and WEI Qing[1] (魏　庆)

1 *State Key Laboratory of Severe Weather, Chinese Academy of Meteorological Sciences, Beijing* 100081

2 *Nanjing Meteorological Radar Open Laboratory, Jiangsu Institute of Meteorological Sciences, Nanjing* 210008

3 *Anhui Weather Modification Office, Hefei* 230031

(Received June 25, 2014; in final form October 8, 2014)

ABSTRACT

Measured differential phase shift $\Phi_{\rm DP}$ is known to be a noisy unstable polarimetric radar variable, such that the quality of $\Phi_{\rm DP}$ data has direct impact on specific differential phase shift $K_{\rm DP}$ estimation, and subsequently, the $K_{\rm DP}$-based rainfall estimation. Over the past decades, many $\Phi_{\rm DP}$ de-noising methods have been developed; however, the de-noising effects in these methods and their impact on $K_{\rm DP}$-based rainfall estimation lack comprehensive comparative analysis. In this study, simulated noisy $\Phi_{\rm DP}$ data were generated and de-noised by using several methods such as finite-impulse response (FIR), Kalman, wavelet, traditional mean, and median filters. The biases were compared between $K_{\rm DP}$ from simulated and observed $\Phi_{\rm DP}$ radial profiles after de-noising by these methods. The results suggest that the complicated FIR, Kalman, and wavelet methods have a better de-noising effect than the traditional methods. After $\Phi_{\rm DP}$ was de-noised, the accuracy of the $K_{\rm DP}$-based rainfall estimation increased significantly based on the analysis of three actual rainfall events. The improvement in estimation was more obvious when $K_{\rm DP}$ was estimated with $\Phi_{\rm DP}$ de-noised by Kalman, FIR, and wavelet methods when the average rainfall was heavier than 5 mm h^{-1}. However, the improved estimation was not significant when the precipitation intensity further increased to a rainfall rate beyond 10 mm h^{-1}. The performance of wavelet analysis was found to be the most stable of these filters.

Key words: de-noising methods, differential phase shift, polarimetric radar-based rainfall estimation

Citation: Hu Zhiqun, Liu Liping, Wu Linlin, et al., 2015: A comparison of de-noising methods for differential phase shift and associated on rainfall estimation. *J. Meteor. Res.*, **29**(2), 315–327, doi:10.1007/s13351-015-4062-6.

1. Introduction

Quantitative precipitation estimation (QPE) is one of the most important applications for weather radar. A comprehensive review of the reliability of weather radar QPE products was conducted by Wilson and Brandes (1979), and it discussed in detail the sources of uncertainty associated with radar-based rainfall estimates. These include calibration, attenuation, anomalous propagation, bright band, beam blockage, ground clutter, spurious returns, and random errors. Moreover, the variability in the relationship between reflectivity (Z) and rainfall rate (R) (Z–R relations) was also discussed. Since that time, there has been great progress in radar hardware and QPE algorithms. Polarimetric radar can measure multiple polarization parameters, including differential reflectivity $Z_{\rm DR}$, specific differential phase $K_{\rm DR}$, and cross-correlation coefficient $\rho_{\rm HV}$ between two orthogonal radar returns. $Z_{\rm DR}$ reflects the median drop diameter. $K_{\rm DR}$ is immune to radar miscalibration, attenuation in precipitation, and beam blockage, while $\rho_{\rm DR}$ can significantly improve the radar data quality, distinguishing rain echoes from the radar signals caused by other scatters such as snow, ground clutter, insects, birds, chaff, etc. (Zrnic and Ryzhkov, 1996; Krajewski

Supported by the National Natural Science Foundation of China (41375038), China Meteorological Administration Special Public Welfare Research Fund (GYHY201306040 and GYHY201306075), and Jiangshu Province Meteorological Administration Beijige Open Research Fund (BJG201201).

*Corresponding author: huzq@cams.cma.gov.cn.

et al., 2010). In recent years, radar meteorologists have paid more attention to the polarimetric radar and its QPE products.

By combining a variety of polarization observational parameters, several QPE algorithms such as $R(Z_{\rm H})$, $R(Z_{\rm H}, Z_{\rm DR})$, $R(Z_{\rm H}, Z_{\rm DR}, K_{\rm DP})$, and $R(K_{\rm DP})$ have been investigated in the past decades (Bringi and Chandrasekar, 2001; Liu et al., 2002; Brandes et al., 2003; Ryzhkov et al., 2005; Hu et al., 2010). However, since polarimetric variables are the difference between horizontal and vertical polarization, their values are one order of magnitude smaller than those measured from only a single polarization direction. Moreover, polarimetric variables are easily influenced by noise, which needs to be removed before generating the polarimetric radar-derived rainfall estimation. For example, Jameson (1991) and Ryzhkov and Zrnić (1995) investigated the relationship between rainfall and polarimetric parameters. Their results indicated that $R(K_{\rm DP}, Z_{\rm DR})$ was better relative to $R(Z_{\rm H})$, $R(Z_{\rm H}, Z_{\rm DR})$, and $R(K_{\rm DP})$ for moderate to heavy rain rates, however, $K_{\rm DP}$ and $Z_{\rm DR}$ needed to be smoothed for greater accuracy of $R(K_{\rm DP}, Z_{\rm DR})$ relative to $R(K_{\rm DP})$. Carey et al. (2000) developed a propagation correction algorithm utilizing the differential propagation phase ($\varPhi_{\rm DP}$) and tested this algorithm using experimental data from the C-band polarimetric radar. Their result showed that the algorithm greatly reduced the error of $R(K_{\rm DP}, Z_{\rm DR})$. Cifelli et al. (2011) presented an optimization algorithm to estimate rainfall on the basis of $Z_{\rm H}$, $Z_{\rm DR}$, and $K_{\rm DP}$, which performed better in both tropical and extratropical regions. Moreover, the US National Severe Storms Laboratory (NSSL) conducted an operational demonstration for the polarimetric radar KOUN, and tested the reliability of KOUN radar QPE for different seasons and rain types using a large dataset. The hourly rain estimate errors using polarimetric QPE were shown to decrease significantly compared to the conventional nonpolarimetric QPE (Ryzhkov et al., 2005). The US National Weather Service (NWS) upgraded the Weather Surveillance Radar-1988 Doppler (WSR-88D) network with polarimetric capability in 2013.

The polarimetric parameter $Z_{\rm DR}$ is easily influenced by radar hardware such as the difference between the two orthogonal polarization directions of antenna gains, rotary joints, waveguides, and receivers (Melnikov et al., 2003). Thus, correction for $Z_{\rm DR}$ system bias is extremely complicated and a small error of $Z_{\rm DR}$ can possibly cause a large bias of $Z_{\rm DR}$-based QPE. In addition, the reliability of $Z_{\rm DR}$-based QPE is greatly affected by attenuation, especially for heavy rainfall. $K_{\rm DP}$, which has been used more widely for polarimetric radar-derived QPE, is the slope of the $\varPhi_{\rm DP}$ profile and is noisy and unstable in measurement, especially for light rain. Thus, pretreatment of $\varPhi_{\rm DP}$ is crucial for $K_{\rm DP}$ estimate quality (Liu et al., 2013).

In recent decades, many $\varPhi_{\rm DP}$ de-noising methods have been developed for increasing the accuracy of $R(K_{\rm DP})$. Sachidananda and Zrnić (1987) presented an analysis of the accuracy of QPE from observed data and a simulation procedure, which indicated that errors caused by sidelobe contamination significantly affect $\varPhi_{\rm DP}$ data. As such, large scale averaging is required to obtain reasonably accurate rain rate estimates. Chandrasekar et al. (1990) focused on the error structure of $K_{\rm DP}$, and simulated random errors in $Z_{\rm H}$, $Z_{\rm DR}$, and $K_{\rm DP}$, which suggested that $R(K_{\rm DP})$ is stable and insensitive to system calibration.

As $K_{\rm DP}$ is crucial in polarimetric radar-derived rain estimates, radar meteorologists have for many years investigated how to obtain accurate $K_{\rm DP}$ data from $\varPhi_{\rm DP}$. An iterative filtering technique has been developed to estimate $K_{\rm DP}$, which can separate both $\varPhi_{\rm DP}$ and the differential backscatter phase shift δ from complicated echoes (Hubbert et al., 1993; Hubbert and Bringi, 1995). Ryzhkov and Zrnic (1996) presented an algorithm that uses $K_{\rm DP}$ exclusively, and suggested that $R(K_{\rm DP})$ can be successfully applied to low rain rates, however, the $\varPhi_{\rm DP}$ fitting interval needs to be adjusted. May et al. (1999) described a $K_{\rm DP}$ estimation algorithm, for which $R(K_{\rm DP})$ produces higher quality data than $R(Z_{\rm H})$ for moderate to high rain rates. Gorgucci et al. (1999, 2000) similarly described an algorithm to correct bias in the estimation of $K_{\rm DP}$ in nonuniform rainfall paths and evaluated $K_{\rm DP}$-based rainfall algorithms for different pathlengths. With the development of polarization radar, and the recent application of a new mathematical method, $\varPhi_{\rm DP}$ and $K_{\rm DP}$ process methods are constantly developed. Wang and Chandrasekar (2009) presented a robust algorithm to process Φ_{DP}, which is able to remain in sync with the spatial gradients of rainfall and produce a high-resolution K_{DP}.

Recently, an extended Kalman filter framework was proposed, which determines rain-rate via a relationship between R, K_{DP}, and Z_{DR} (Schneebeli and Berne, 2012; Grazioli et al., 2014). Vulpiani et al. (2012) demonstrated that $R(K_{\mathrm{DP}})$ has a more seasonal relationship than $R(Z_{\mathrm{H}})$, except for the analyzed winter storm. To estimate high-resolution K_{DP}, Hu et al. (2012) developed an algorithm that can smoothen Φ_{DP} as well as a synthetic $Z_{\mathrm{H}}/K_{\mathrm{DP}}$-based rainfall estimation method. They showed that the accuracy of $R(Z_{\mathrm{H}}, K_{\mathrm{DP}})$ is higher than the traditional $R(Z_{\mathrm{H}})$ method when the rain rate is larger than 5 mm h^{-1}. Giangrande et al. (2013) presented an application of linear programming for physical retrievals, in order to process measured Φ_{DP} by developing realistic physical constraints for the monotonicity and polarimetric radar self-consistency. Hu and Liu (2014) introduced wavelet analysis into the Φ_{DP} de-noising process and further addressed a Φ_{DP} penalty threshold strategy based on the attribution of weather echoes.

A variety of Φ_{DP} de-noising methods are used extensively, yet there remains a lack of comprehensive comparative analysis of these de-noising methods and their influences on K_{DP}-based QPE. In the present study, several new Φ_{DP} de-noising methods are introduced in Section 2. In Section 3, a simulated noisy Φ_{DP} profile is constructed and filtered with these and other traditional methods. The bias is compared where K_{DP} is calculated from the simulated Φ_{DP} with various de-noising methods. In Section 4, an observed Φ_{DP} radial profile is selected as an example to determine the differences between raw and de-noised data. In Section 5, K_{DP}-based rainfall estimates are verified against rain gauge measurements to evaluate the ability of the Φ_{DP} de-noising methods. Finally, the conclusions and discussion are given in Section 6.

2. Description of de-noising methods

With exception of the traditional running average and median filter methods, a host of new algorithms have also been applied into the Φ_{DP} de-noising process. The following three methods, finite-impulse response filter (FIR), Kalman filter, and wavelet analysis, have been proved effective in removing Φ_{DP} noise.

2.1 *Finite-impulse response filter*

An FIR filter system function $H(z)$ may be given as follows,

$$H(z) = \sum_{n=0}^{m-1} b_k Z^{-n}, \qquad (1)$$

where coefficients b_0, b_1, $\cdots$, b_{m-1} represent the system unit impulse response $h(0)$, $h(1)$, $\cdots$, $h(m-1)$; n is the time or the coordinates in space or distance, and indicates the ordinal number of gates in a radar radial; m is the filter window width, and here also refers to the smoothing gate number in a radar radial. After a signal $x(n)$ is processed with FIR, the output $y(n)$ is shown as

$$y(n) = x(n)^{*}h(n), \qquad (2)$$

where "*" denotes the convolution. The FIR system can be calculated from the following difference equation,

$$y(n) = b_0x(n) + b_1x(n-1) + b_2x(n-2) + \cdots + b_mx(n-m) = \sum_{k=0}^{m} b_kx(n-k). \qquad (3)$$

Proakis and Manolakis (1988) used symmetric 20th-order associated coefficients in the complex variable Z (Table 1). This method was used to smooth the Φ_{DP} radial profile for both the German Aerospace Research Institute's C-band radar and the NCAR CP-2 radar (Hubbert et al., 1993; Hubbert and Bringi, 1995). In this study, the same coefficients in Table 1 were substituted into b_k in Eq. (3) to smooth the Φ_{DP} radial profile.

2.2 *Kalman filter*

For the Kalman filter, the observational data are regarded as an output from a state equation and the least mean square error is used as an optimal estimation criterion to estimate the state vector of the origi-

Table 1. FIR filter coefficients

Z order	Coefficient	Z order
Z^{0}	1.625807356e–2	Z^{-20}
Z^{-1}	2.230852545e–2	Z^{-19}
Z^{-2}	2.896372364e–2	Z^{-18}
Z^{-3}	3.595993808e–2	Z^{-17}
Z^{-4}	4.298744446e–2	Z^{-16}
Z^{-5}	4.971005447e–2	Z^{-15}
Z^{-6}	5.578764970e–2	Z^{-14}
Z^{-7}	6.089991897e–2	Z^{-13}
Z^{-8}	6.476934523e–2	Z^{-12}
Z^{-9}	6.718151185e–2	Z^{-11}
Z^{-10}	6.800100000e–2	

nal system. We assume that random signals a and V are defined as the process and measurement noises, which are mutually independence white noises with Gauss distributions of $p(a) \sim N(0,\boldsymbol{Q})$ and $p(\boldsymbol{V}) \sim N(0,\boldsymbol{S})$, respectively. Here $\boldsymbol{Q}$ and $\boldsymbol{S}$ are the covariance matrixes. To remove the noise of Φ_{DP}, the process and measurement equations of the Kalman filter are presented as (He et al., 2009)

$$\boldsymbol{X}(r) = A\boldsymbol{X}(r-1) + \boldsymbol{B}a(r-1), \tag{4}$$

$$\boldsymbol{P}(r) = C\boldsymbol{X}(r) + \boldsymbol{V}(r), \tag{5}$$

$$\boldsymbol{X}(r) = \begin{bmatrix} \Phi_{\mathrm{DP}}(r) \\ K_{\mathrm{DP}}(r) \end{bmatrix}, \tag{6}$$

$$\boldsymbol{A} = \begin{bmatrix} 1 & r \\ 0 & r \end{bmatrix}, \tag{7}$$

$$\boldsymbol{B} = \begin{bmatrix} r^2/2 \\ r \end{bmatrix}, \tag{8}$$

$$\boldsymbol{C} = [1 \qquad 0], \tag{9}$$

where the definitions of variables in Eqs. (4)–(9) are listed in Table 2.

Table 2. Definition of the variables in Eqs. (4)–(9)

Variable	Meaning
$\boldsymbol{X}(r)$	System state
$\boldsymbol{P}(r)$	Measured value
r	At the distance r (unit: km)
$\boldsymbol{A}$	System matrix
$\boldsymbol{B}$	State transition matrix
$\boldsymbol{C}$	Measured matrix
$a(r)$	Process noise, Gaussian distribution with zero mean and $\boldsymbol{Q}$ variance, i.e., $p(a) \sim \boldsymbol{N}(0,\boldsymbol{Q})$
$\boldsymbol{V}(r)$	Measurement noise, Gaussian distribution with zero mean and $\boldsymbol{S}$ variance, i.e., $p(\boldsymbol{V}) \sim \boldsymbol{N}(0,\boldsymbol{S})$

2.3 Wavelet analysis

Wavelet analysis can localize a signal in both the time and frequency domains. It performs multi-scale analysis using signal zoom and transform, in which the information of signal is kept well. Thus, it has rapidly become a significant technology in signal processing. Hu and Liu (2014) employed this analysis to remove the noise of Φ_{DP}, and proposed a Φ_{DP} process strategy based on the weather echo attributions. The wavelet de-noising process generally includes the following steps:

(1) Deconstruction: a signal is deconstructed into approximate and detailed components of several levels by a selected wavelet function.

(2) De-noising process: the coefficients of components detailed in each level are suppressed by a selected threshold strategy.

(3) Reconstruction: the signal is reconstructed by approximation and using the processed detailed coefficients with a selected threshold function.

Based on Hu and Liu (2014), in this study, the db5 wavelet function is used to deconstruct a signal into five levels. The detailed coefficients are suppressed by the Φ_{DP} penalty threshold strategy, and the signal is reconstructed by soft function.

3. Evaluation with a simulated Φ_{DP} profile

To quantitatively compare the performance of K_{DP} when Φ_{DP} is de-noised with alternative methods, a radar radial profile is simulated, which passes through two convective cloud cells that were assumed of a gamma drop size distribution (Ulbrich, 1983, Chandrasekar et al., 1990; Scarchilli et al., 1993) as follows:

$$N_w(D) = N_0 D^{\mu} \mathrm{e}^{-(3.67+\mu)D/D_0}, \quad (10)$$

where N_w is the raindrop number for one unit volume and size interval, D is the equivalent volume diameter of raindrops (mm), N_0 is the concentration parameter which is assumed to be 8×10^3 mm^{-1} m^{-3}, μ is the distribution parameter (set to zero for this study), and D_0 is the median volume diameter, which is assumed to have the following distribution,

$$D_0(r) = D_{\max} \exp\left[-2\ln 2\left(\frac{r - r_{\max}/2}{r_{\max}}\right)^2\right], \quad (11)$$

where $D_{\max}$ represents the maximum equivalent diameter of raindrops (assumed to be 0.2 cm); $r_{\max}$ is the diameters of two cells, for which the first is set to 30 km and the next 15 km; and r is the distance of a raindrop from the center of each cell. We set the radar wavelength to 5.6 cm and the gate width to 150 m. Therefore, there are 300 gate measurements as the beam propagates through the simulated rain area. Particle scattering is calculated using the extended boundary condition method which considers the relationship between the drop size and the ellipticity (Liu et al., 1989).

Figure 1 shows the simulated radar radial profiles of Z_{H}, Z_{DR}, Φ_{DP}, and K_{DP}. The two symmetrical rain cells are clearly evident in the profiles. As a result of attenuation, the radial profile of Z_{H} is not symmetric to the center of the two convective cells. Z_{H} values behind the centers are obviously smaller than those in front. The profile of Z_{DR} reveals a similar behavior, for the same reason. However, Φ_{DP} is immune to attenuation and the profile of Φ_{DP} increases monotonically from zero to 83.35°. The K_{DP} curve derived from Φ_{DP} shows symmetrical features for the two cells and changes from 0.07° to 0.45° km^{-1}, with similar fluctuations in Z_{H} and Z_{DR}.

In order to simulate a measured Φ_{DP} profile, white noise with a signal to noise ratio (SNR) of 25 dB was added. Figure 2 shows the noisy Φ_{DP} profile and the de-noised profiles with mean filters (window

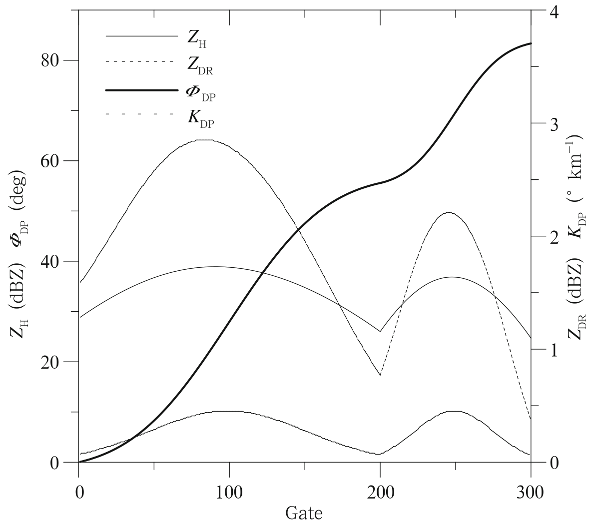

Fig. 1. The simulated radar radial profiles of Z_{H}, Z_{DR}, Φ_{DP}, and K_{DP}.

widths of 7 and 13 points, respectively), median (7 and 13 points, respectively), FIR, Kalman, and wavelet methods. The curves de-noised by the complicate FIR, Kalman, and wavelet methods are obviously smoother than those by the traditional mean and median methods. Namely, the FIR, Kalman, and wavelet methods have better de-noised effects than do traditional methods.

Using the least squares fitting method, K_{DP} is estimated with 13 consecutive Φ_{DP} in Fig. 2. The corresponding K_{DP} profiles are displayed in Fig. 3. Due to the noise and the various de-noised methods, the profiles of K_{DP} fluctuate to varying degrees. The maximum bias of K_{DP} is 0.57° km^{-1} for the procedure without any de-noising (Fig. 3a). After de-noising, the maximum bias of K_{DP} (Figs. 3b–h) is 0.44, 0.38, 0.46, 0.25, 0.20, 0.14, and 0.06° km^{-1}, respectively. The profiles of K_{DP} filtered by FIR, Kalman, and wavelet methods (Figs. 3g–h) are also found more similar to the true K_{DP} (Fig. 1) than the profiles filtered by the traditional methods (Figs. 3b–e). In particular, the wavelet method in Fig. 3h proves the most similar.

In order to quantitatively evaluate the Φ_{DP} de-noising effect on the K_{DP} estimate, the mean absolute error ε and mean relative bias d are defined as

$$\varepsilon = \frac{1}{G}\sum_{n=1}^{G} |K'_{\mathrm{DP}}(n) - K_{\mathrm{DP}}(n)|, \quad (12)$$

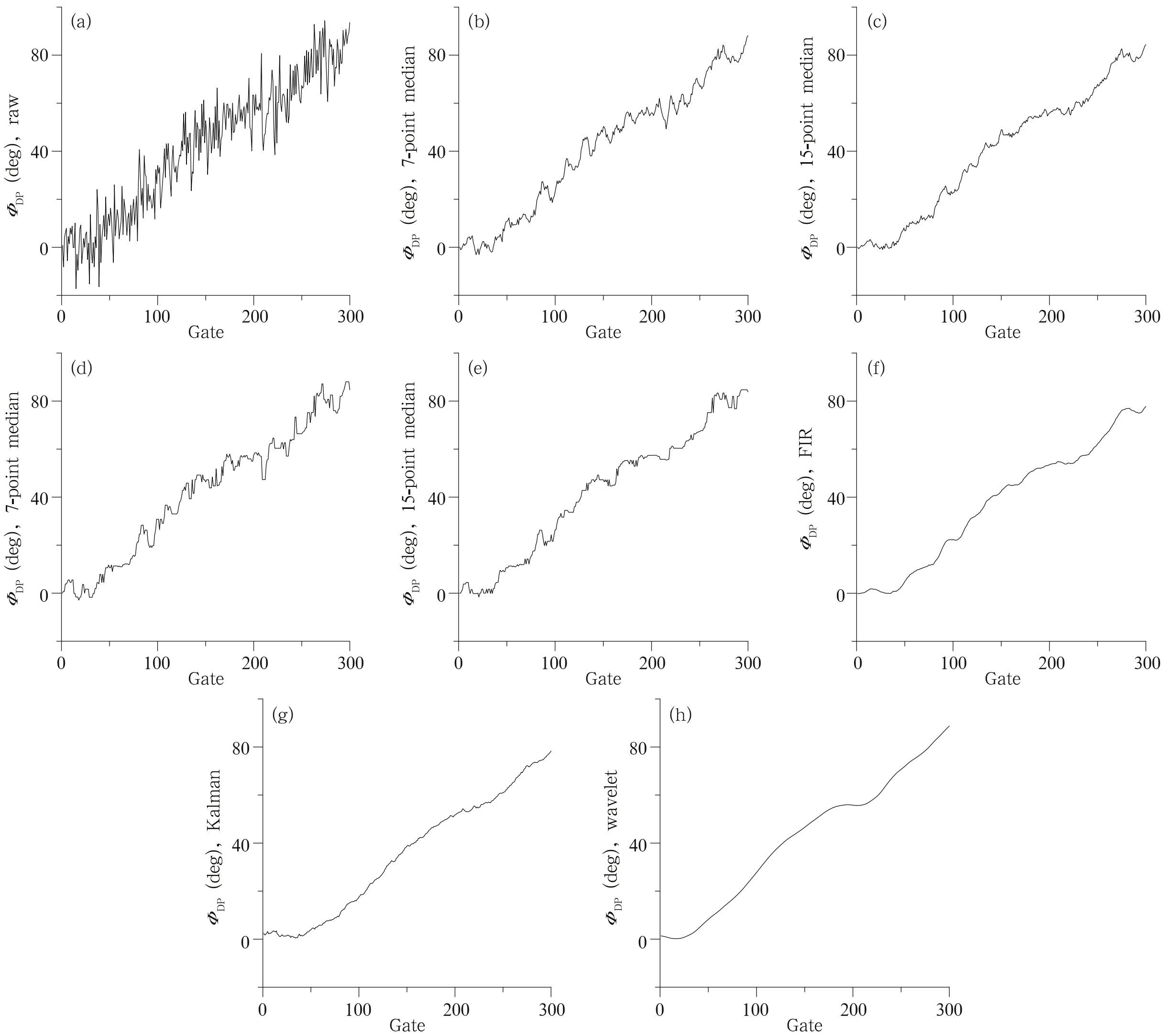

Fig. 2. The noisy $\Phi_{\rm DP}$ profile (a) and the de-noised profiles by (b) and (c) 7- and 13-point mean, (d) and (e) 7- and 13-point median, (f) FIR, (g) Kalman, and (h) wavelet filters, respectively.

$$d = \frac{1}{G}\sum_{n=1}^{G}\frac{|K'_{\rm DP}(n) - K_{\rm DP}(n)|}{K_{\rm DP}(n)} \times 100\%, \qquad (13)$$

where $K'_{\rm DP}$ and $K_{\rm DP}$ represent the fitting values in Fig. 2 and the simulated value in Fig. 1, respectively, n is the gate ordinal number, and G is 287, the total number of fitted $K_{\rm DP}$, i.e., the total $\Phi_{\rm DP}$ gate number of 300 minus a fitting width of 13.

The $K_{\rm DP}$ mean absolute error and mean relative bias results are listed in Table 3. Without de-noising, ε (0.19) and d (78.40%) are the largest among those listed in Table 3, indicating that all the methods selected in this study de-noise $K_{\rm DP}$ and more closely represent the simulated $K_{\rm DP}$. The mean and median filters with more window points are an improvement, compared to those with fewer points. However, this does not suggest that the more points the better. The number of points of a window needs to be carefully selected based on the balance between smoothness and feature maintenance. The variables ε and d of FIR, Kalman, and wavelet methods are smaller than those generated by the traditional methods, with the error from the wavelet method the smallest.

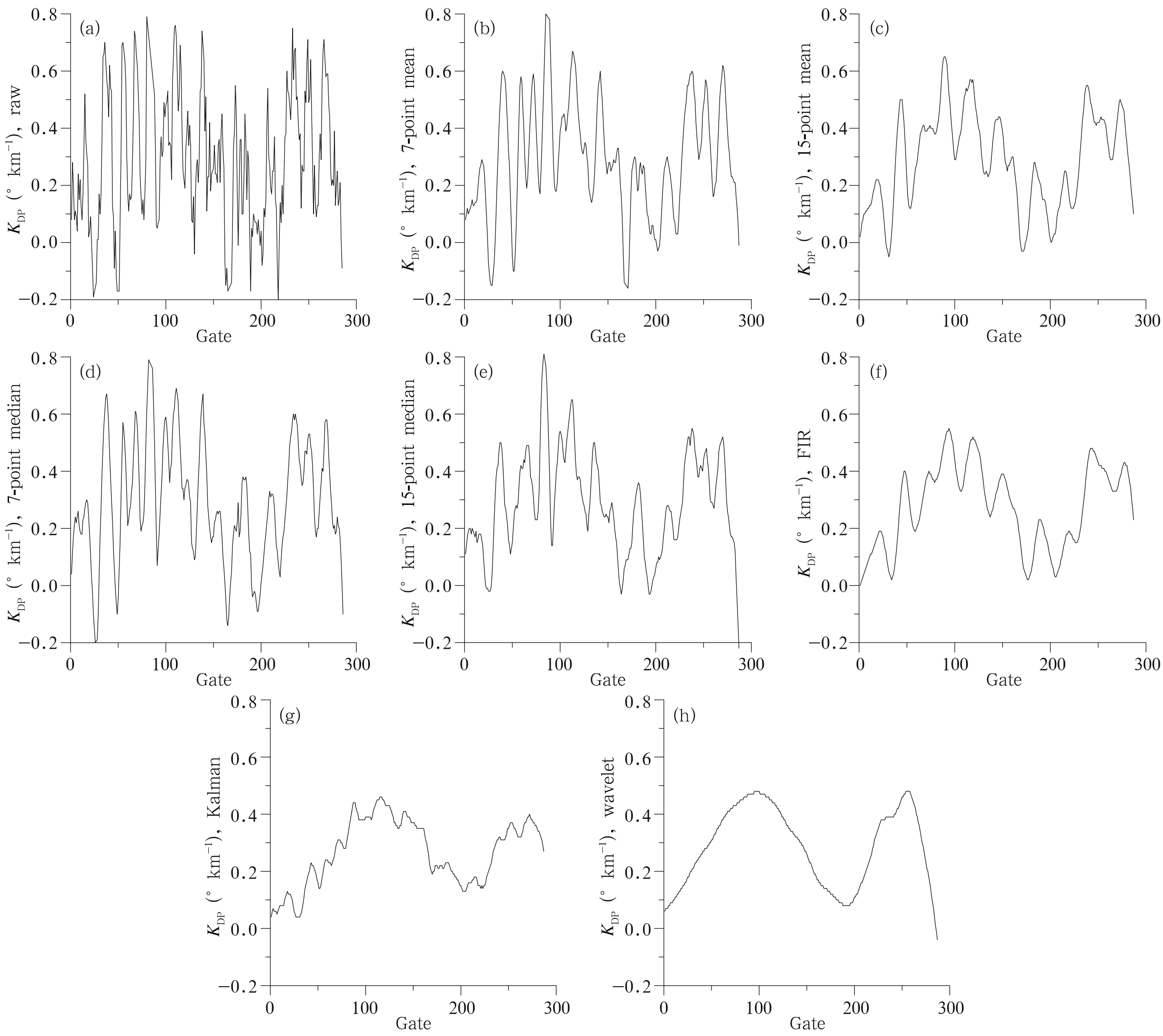

Fig. 3. The $K_{\rm DP}$ profile of (a) without de-noising, and with (b) 7- and (c) 13-point mean, (d) 7- and (e) 13-point median, (f) FIR, (g) Kalman, and (h) wavelet filters.

Table 3. The $K_{\rm DP}$ mean absolute error and mean relative bias of each de-noising method

Methods	Noise	Mean 7	Mean 13	Median 7	Median 13	FIR	Kalman	Wavelet
ε	0.19	0.13	0.08	0.14	0.10	0.07	0.08	0.03
d (%)	78.40	54.30	37.36	63.37	43.65	32.72	33.92	12.45

4. Comparison with real $\Phi_{\rm DP}$ radial profile

The following representative real $\Phi_{\rm DP}$ radial profile at 0.5° elevation and 62.0° azimuth was detected with the mobile C-band dual polarimetric weather radar (POLC), which transmitted and received horizontal and vertical polarization signals simultaneously, at 0804 BT (Beijing Time) 25 June 2013 in Dingyuan, Anhui Province. The main characteristics of the radar, which operated at a frequency of 5.43 GHz and a 150-m gate width, are summarized in Table 4.

Figure 4 shows the profiles of raw data and de-noised $\Phi_{\rm DP}$ data from the previously mentioned methods. The corresponding $K_{\rm DP}$ are displayed in Fig. 5.

Table 4. Main characteristics of POLC radar

Parameter	Value
Antenna diameter	3.2 m
Gain	40 dB
Beam width	1.2°
First side lobe	< –25 dB
Isolation	> 40 dB
Wavelength	5.5 cm
Pulse width	1.0/0.5 μs
Peak power	$\geqslant$ 250 kW
PRF	300–1200 Hz
Polarization	Horizontal and vertical
Minimum detectable signal	$\leqslant$ –109 dBm
Receiver noise figure	$\leqslant$ 3.0 dB
Receiver dynamic range	> 85 dB
Observation range	150 km

Note that the scale of y-axis in Fig. 5a is 10 times larger than in Figs. 5b–h. Hence, the $K_{\rm DP}$ errors are very large if $\Phi_{\rm DP}$ data are not preprocessed before $K_{\rm DP}$ fitting. $K_{\rm DP}$ derived by the Kalman method (Fig. 5g) is smoother than by other methods, which implies that more detailed spatial features may be lost by the de-noise procedure. The FIR method (Fig. 5f) exhibits an evident boundary effect, which will influence the $K_{\rm DP}$ values at the echo boundaries. In addition, the traditional mean and median methods are less smooth. The wavelet analysis, on the other hand, is sufficiently smooth, and at the same time preserves enough detail information of weather echo, which helps

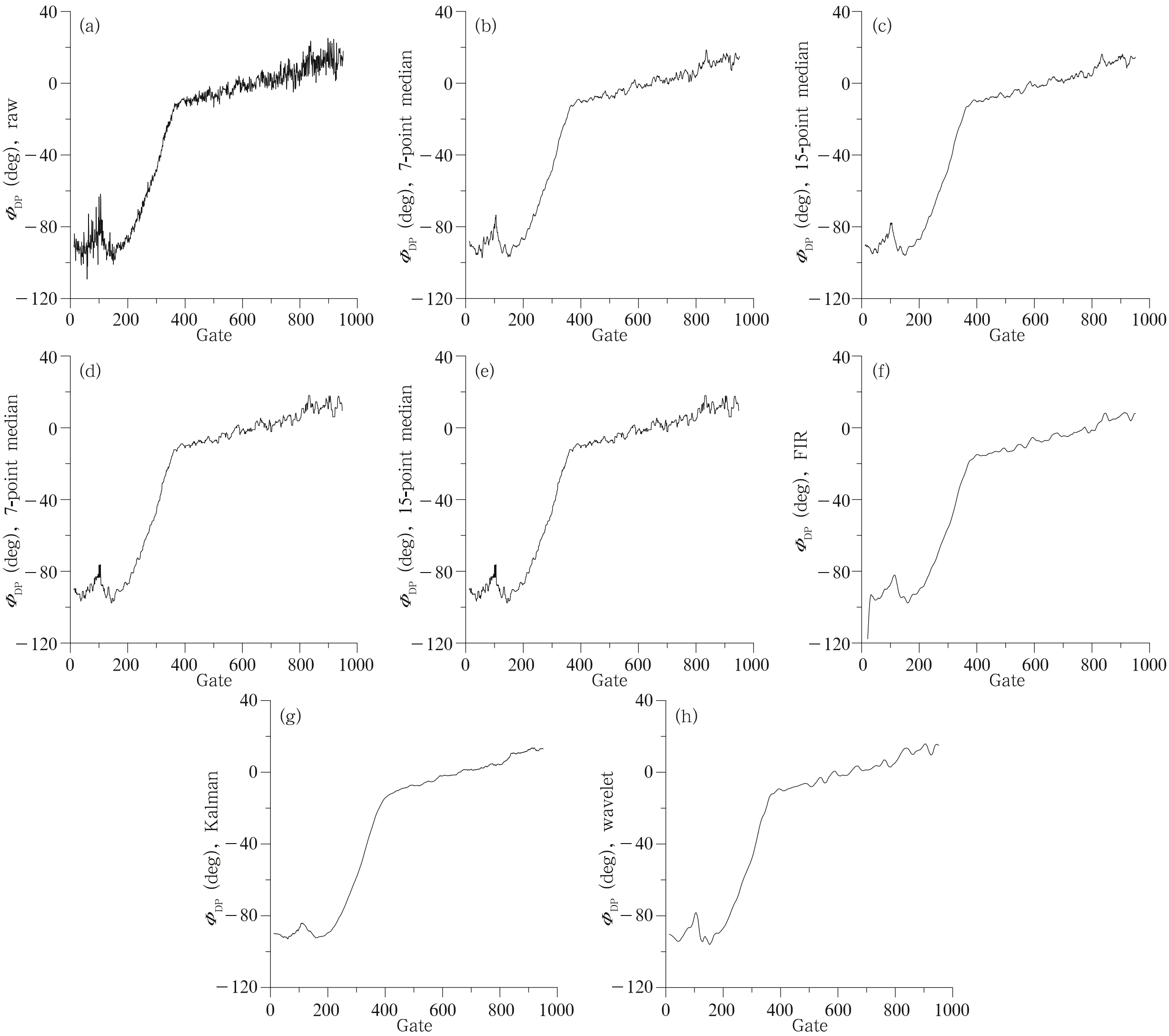

Fig. 4. As in Fig. 2, but for raw $\Phi_{\rm DP}$ data at 0.5° elevation and 62.0° azimuth detected at 0804 BT 25 June 2013 in Dingyuan, Anhui Province.

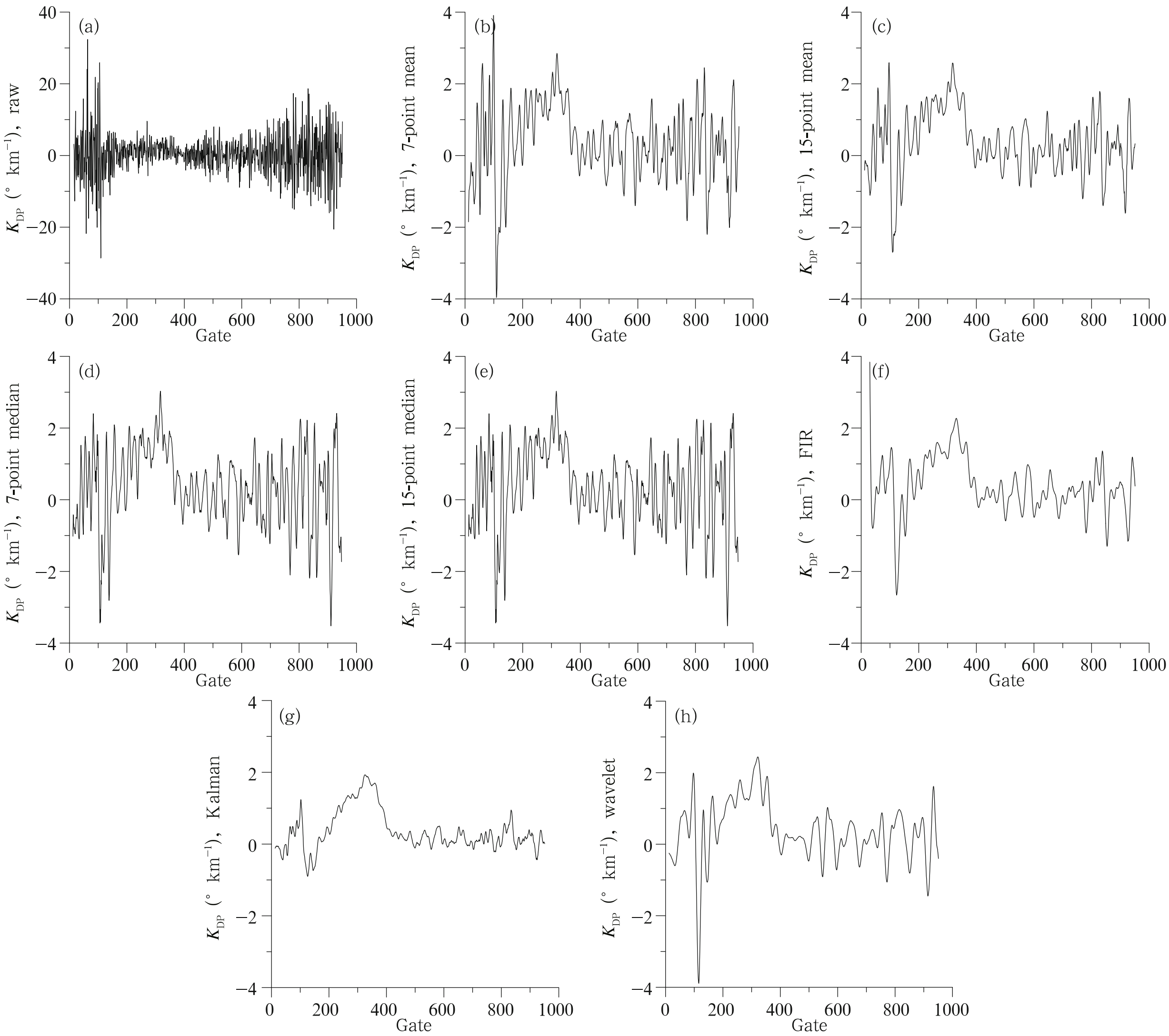

Fig. 5. As in Fig. 3, but the $K_{\rm DP}$ profiles were obtained by using the $\Phi_{\rm DP}$ data in Fig. 4. Note that the scale of y-axis in (a) is 10 times larger than others.

effectively locate the strong convection and precipitation. Figure 6 is the corresponding plan position indicators (PPIs) of $Z_{\rm H}$ and $\Phi_{\rm DP}$, and Fig. 7 is the $K_{\rm DP}$ PPIs corresponding to Fig. 4. $K_{\rm DP}$ noise in Fig. 7a is decreased by the $\Phi_{\rm DP}$ de-noising (Figs. 7b–h). The $K_{\rm DP}$ PPIs of traditional mean and median methods (Figs. 7b–e) barely differ from the visual views. The FIR, Kalman, and wavelet methods (Figs. 7f–h) are relatively smooth compared to the traditional methods, yet the Kalman method (Fig. 7g) is too smooth for $K_{\rm DP}$ to locate the strong echoes that are easily seen in $Z_{\rm H}$ (Fig. 6a) and other $K_{\rm DP}$ PPIs. For example, in Fig. 4, the average reflectivity is 42.15 dBZ in the strong echo area from gates 183 to 352, and the average value 1.17° km^{-1} of $K_{\rm DP}$ using the Kalman method is the smallest (Table 5).

5. QPE results of three real cases

In order to further verify the influence on $K_{\rm DP}$-based rainfall estimation, three large-scale rainfall processes during 0200–0800 BT 25 June, 0900–1700 BT

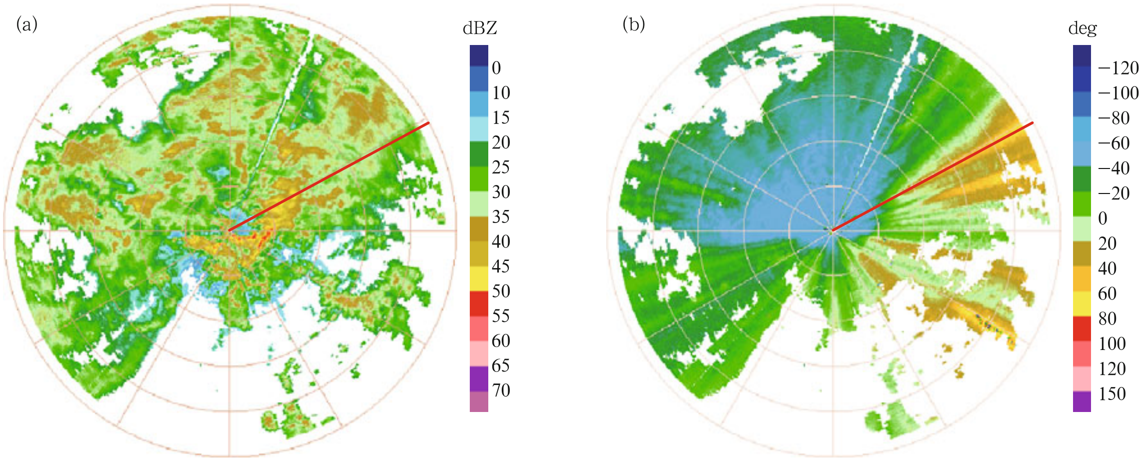

Fig. 6. (a) $Z_{\rm H}$ (dBZ) and (b) $\Phi_{\rm DP}$ (deg) PPIs observed at 0.5° elevation and 62.0° azimuth detected at 0804 BT 25 June 2013 in Dingyuan, Anhui Province. The red line denotes location of the radial profile in Fig. 4. Range rings are 30-km apart.

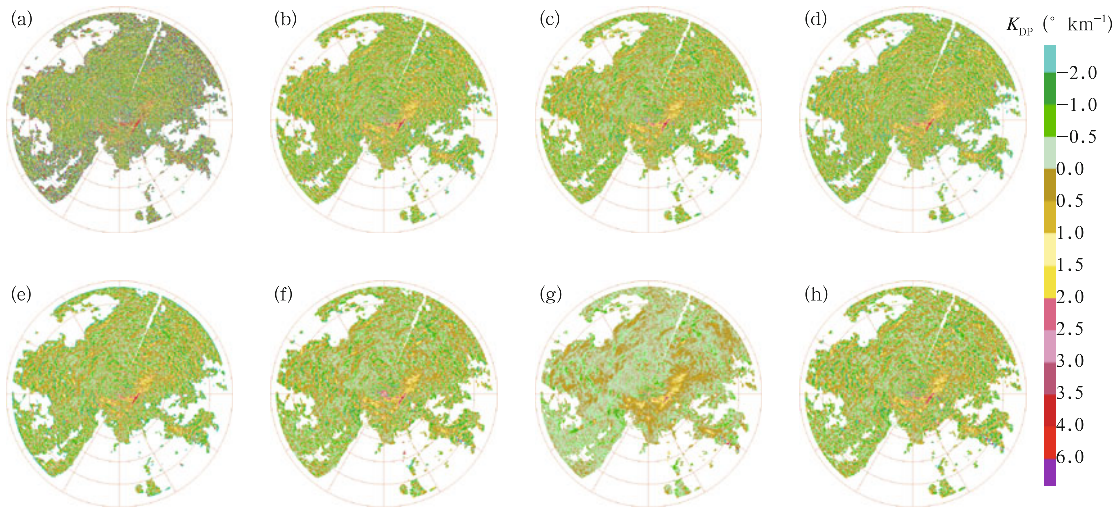

Fig. 7. $K_{\rm DP}$ PPIs fitted by (a) raw $\Phi_{\rm DP}$ in Fig. 6b, and (b–h) de-noised $\Phi_{\rm DP}$.

Table 5. Average values of $Z_{\rm H}$, raw $K_{\rm DP}$, and $K_{\rm DP}$ de-noised with various methods in the strong echo area from gate 183 to 352

Average	Average $K_{\rm DP}$ (° km^{-1})							
$Z_{\rm H}$ (dBZ)	Raw	Mean 7	Mean 13	Median 7	Median 13	FIR	Kalman	Wavelet
42.15	1.39	1.40	1.40	1.43	1.43	1.27	1.17	1.39

5 July, and 0900–1700 BT 7 July 2013 are analyzed, and their $\Phi_{\rm DP}$ values are de-noised with various methods. The hourly rainfall is measured by 160 rain gauges around the radar within 70 km. $Z_{\rm H}$ is pre-processed by attenuation correction (Hu et al., 2012), and the $Z_{\rm H}$-based QPE equation is taken as

$$\begin{cases} Z_{\rm H} = 200R_{\rm r}^{1.6}, & Z_{\rm H} \leqslant 37 \text{ dBZ} \\ Z_{\rm H} = 300R_{\rm r}^{1.4}, & Z_{\rm H} > 37 \text{ dBZ} \end{cases}, \tag{14}$$

and the K_{DP}-based QPE equation is (Liu et al., 2002):

$$R_{\mathrm{r}} = 28.76 K_{\mathrm{DP}}^{0.779}. \tag{15}$$

In order to analyze the accuracy of QPE, the normalized error (NE) is defined as

$$\mathrm{NE} = \frac{\frac{1}{M}\sum_{i=1}^{M}|R_{\mathrm{r}} - R_{\mathrm{g}}|}{\frac{1}{M}\sum_{i=1}^{M}R_{\mathrm{g}}} \times 100\%, \tag{16}$$

where R_{r} and R_{g} represent radar estimated and gauge measured rainfall, respectively, and M represents the number of qualified data pairs when both the estimated and measured rainfall are larger than 0.0 mm.

The normalized errors (NEs) of $R(Z_{\mathrm{H}})$ and $R(K_{\mathrm{DP}})$ are listed in Table 6, in which $<R_{\mathrm{g}}>$ represents the average rainfall measured with all gauges, and the bold numbers indicate the minimum NE of $R(K_{\mathrm{DP}})$ with different de-noising methods. As expected $R(Z_{\mathrm{H}})$ is the best estimator when all data pairs are statistically counted, regardless of rainfall intensity (Hu et al., 2010, 2012). When only R_{g} values greater than 5, 10, 15 mm h^{-1} are considered, the advantage of K_{DP}-based estimation is evident: the heavier the precipitation, the higher the accuracy of K_{DP}-based QPE. The SNR of the echo signal increases with greater rainfall, and the quality of the K_{DP} data improves rapidly. Even without any pretreatment, the K_{DP}-based estimates have improved 10.61% (49.09% minus 38.48%) and 19.85% (51.88% minus 32.03%), in comparison to Z_{H}-based methods, when the average rainfall is heavier than 10 and 15 mm h^{-1} in Table 6, respectively. In Table 6, the wavelet method is the best of these de-noising methods. When the average rainfall is larger than 5 mm h^{-1}, after de-noising, the NE of $R(K_{\mathrm{DP}})$ decreases from 55.41% (raw K_{DP}-based estimates) to a minimum of 36.30% (Kalman method), i.e., the NE of $R(K_{\mathrm{DP}})$ has improved from –7.43% to 11.68% of $R(Z_{\mathrm{H}})$. In addition, the filter window widths, i.e., 7 or 13 points of Φ_{DP}, of traditional mean and median filters seem to have little influence on the results of K_{DP}-based QPE in all three cases.

Table 6. Normalized errors (NEs) of Z_{H}- and K_{DP}-based rainfall estimation with raw and various de-noising methods

Rain rate	Data pair	$<R_{\mathrm{g}}>$	NE (%)								
(mm h^{-1})	number	mm h^{-1}	$R(Z_{\mathrm{H}})$	Raw	Mean 7	Mean 13	Median 7	Median 13	FIR	Kalman	Wavelet
>0	2483	5.06	104.88	2934.00	651.78	736.56	768.88	695.98	588.27	429.21	1050.21
>5	780	14.02	47.98	55.41	41.48	40.35	43.40	42.52	36.48	36.30	37.81
>10	428	19.57	49.09	38.48	31.98	30.54	33.89	32.32	31.39	31.31	30.42
>15	255	25.29	51.88	32.03	29.63	29.70	30.64	31.05	31.05	30.84	29.57

6. Discussion and summary

Since the polarimetric variable is one order of magnitude smaller than those measured from a polarization direction, they are easily influenced by noise. This is particularly the case in low SNR conditions for which the useful echo information is always submerged in noise. As K_{DP} is one of the polarization parameters, how Φ_{DP} measurements are processed and obtaining better K_{DP} will directly influence the accuracy of K_{DP}-based QPE. In recent decades, many types of Φ_{DP} preprocessing methods have been employed; however, the specific effects of these de-noising methods and K_{DP}-based QPE are yet to undergo comprehensive comparative analysis.

In this paper, the Φ_{DP} filtering effect with various common methods is assessed and compared by using numerical simulation, and finally demonstrated by real Φ_{DP} radial. The K_{DP}-based rainfall estimates are also evaluated by refitting K_{DP} to further analyze the influence of the different Φ_{DP} de-noising methods.

Φ_{DP} de-noising clearly reduced the errors of $R(K_{\mathrm{DP}})$, with the improvement more obvious when Φ_{DP} de-noising used the more complicated Kalman, FIR, and wavelet methods, and the rainfalls were heavier than 5 mm h^{-1}. However, for heavier precipitation (R > 10 mm h^{-1}), with an increased SNR, the differences between these methods are not significant.

Therefore, for strong precipitation, the filtering method is not the primary consideration. Since the efficiency of the complicated Kalman, FIR, and wavelet methods is significantly lower than that of the traditional methods for different precipitation types and rain rates, an efficient $\Phi_{\rm DP}$ de-noising program needs to be deliberately designed. For instance, the threshold value of average $Z_{\rm H}$ in a radial can be set to determine whether the radial data are de-noised with fast traditional methods or more complicated ones.

In addition, it is found that the filter window width of traditional filters on $\Phi_{\rm DP}$ had less impact on $K_{\rm DP}$-based QPE in the three large-scale rainfall processes. In other words, if the rain rate is greater than 10 mm h^{-1}, these de-noising methods are basically similar. Overall, the performance of the wavelet method is better than other methods. Nonetheless, these results need to be appropriately verified with more observational data, especially for convective cloud rainfall processes.

It has been found that the value of $K_{\rm DP}$ is less representative than those of $Z_{\rm H}$ and $Z_{\rm DR}$, as $K_{\rm DP}$ is fitted by a number of gates over a gauge, and $Z_{\rm H}$ and $Z_{\rm DR}$ are detected only over a gate width. As such, the accuracy of $Z_{\rm H}$- and $Z_{\rm DR}$-based rainfall estimations should be higher than the $K_{\rm DP}$-based estimation. Aside from the algorithm and radar system errors, precipitation is a complex dynamic, thermodynamic, and microphysical process. Due to the air flow, time and space are needed before the echoes detected by radar are transformed into rainfall measured with ground gauges. The results in this paper further suggest that the accuracy of $K_{\rm DP}$-based rainfall estimation is higher than the $Z_{\rm H}$-based estimation for heavy rainfall ($R > 10$ mm h^{-1}), and that after $\Phi_{\rm DP}$ de-noising, the accuracy of $K_{\rm DP}$-based QPE is more accurate than $Z_{\rm H}$-based QPE, even for light to moderate rain ($R > 5$ mm h^{-1}).

REFERENCES

Brandes, E. A., G. Zhang, and J. Vivekanandan, 2003: An evaluation of a drop distribution–based polarimetric radar rainfall estimator. *J. Appl. Meteor.*, **42**, 652–660.

Bringi, V. N., and V. Chandrasekar, 2001: *Polarimetric Doppler Weather Radar: Principles and Applications*. Cambridge University Press, Cambridge, 635 pp.

Carey, L. D., S. A. Rutledge, D. A. Ahijevych, et al., 2000: Correcting propagation effects in C-band polarimetric radar observations of tropical convection using differential propagation phase. *J. Appl. Meteor.*, **39**, 1405–1433.

Chandrasekar, V., V. N. Bringi, N. Balakrishnan, et al., 1990: Error structure of multi-parameter radar and surface measurements of rainfall. Part III: Specific differential phase. *J. Atmos. Oceanic Technol.*, **7**, 621–629.

Cifelli, R., V. Chandrasekar, S. Lim, et al., 2011: A new dual-polarization radar rainfall algorithm: Application in Colorado precipitation events. *J. Atmos. Oceanic Technol.*, **28**, 352–364.

Giangrande, S. E., R. McGraw, and L. Lei, 2013: An application of linear programming to polarimetric radar differential phase processing. *J. Atmos. Oceanic Technol.*, **30**, 1716–1729.

Gorgucci, E., G. Scarchilli, and V. Chandrasekar, 1999: Specific differential phase estimation in the presence of nonuniform rainfall medium along the path. *J. Atmos. Oceanic Technol.*, **16**, 1690–1697.

Gorgucci, E., G. Scarchilli, and V. Chandrasekar, 2000: Practical aspects of radar rainfall estimation using specific differential propagation phase. *J. Appl. Meteor.*, **39**, 945–955.

Grazioli, J., M. Schneebeli, and A. Berne, 2014: Accuracy of phase-based algorithms for the estimation of the specific differential phase shift using simulated polarimetric weather radar data. *IEEE Trans. Geosci. Remote Sens.*, **11**, 763–767.

He Yuxiang, Lü Daren, Xiao Hui, et al., 2009: Attenuation correction of reflectivity for X-band dual polarization radar. *Chinese J. Atmos. Sci.*, **33**, 1027–1037. (in Chinese)

Hu Zhiqun, Liu Liping, Chu Rongzhong, et al., 2010: Study of different attenuation correction methods in association with rainfall estimation for X-band polarimetric radars. *Acta Meteor. Sinica*, **24**, 602–613.

Hu Zhiqun, Liu Liping, and Wang Lirong, 2012: A quality assurance procedure and evaluation of rainfall estimates for C-band polarimetric radar. *Adv. Atmos. Sci.*, **29**, 144–156.

Hu Zhiqun and Liu Liping, 2014: Applications of wavelet analysis in differential propagation phase shift data de-noising. *Adv. Atmos. Sci.*, **31**, 825–835.

Hubbert, J. V., V. Chandrasekar, V. N. Bringi, et al., 1993: Processing and interpretation of coherent dual-polarized radar measurements. *J. Atmos. Oceanic Technol.*, **10**, 155–164.

Hubbert, J. V., and V. N. Bringi, 1995: An iterative filtering technique for the analysis of copolar differential phase and dual-frequency radar measurements. *J. Atmos. Oceanic Technol.*, **12**, 643–648.

Jameson, A. R., 1991: Polarization radar measurements in rain at 5 and 9 GHz. *J. Appl. Meteor.*, **30**, 1500–1513.

Krajewski, W. F., G. Villarini, and J. A. Smith, 2010: Radar-rainfall uncertainties. *Bull. Amer. Meteor. Soc.*, **91**, 87–94.

Liu Liping, Xu Baoxiang, and Cai Qiming, 1989: The effects of attenuation by precipitation and sampling error on measuring accuracy of 713 type dual linear polarization radar. *Plateau Meteorology*, **8**, 181–188. (in Chinese)

Liu Liping, Ge Renshen, and Zhang Peiyuan, 2002: A study of method and accuracy of rainfall rate and liquid water content measurements by dual linear polarization Doppler radar. *Chinese J. Atmos. Sci.*, **26**, 709–720. (in Chinese)

Liu, L. P., G. L. Wang, Z. Q. Hu, et al., 2013: *Multiple Radar Integration Technology and Application to Heavy Rainfall Monitoring in Southern China*. China Meteorological Press, Beijing, 92–104. (in Chinese)

May, P., T. D. Keecnan, D. Zrnic, et al., 1999: Polarimetric radar measurements of tropical rain at 5-cm wavelength. *J. Appl. Meteor.*, **38**, 750–765.

Melnikov, V. M., D. S. Zrnic, R. J. Doviak, et al., 2003: Calibration and Performance Analysis Of NSSL's Polarimetric WSR-88D. NOAA/NSSL Rep., 77 pp.

Proakis, J. G., and D. G. Manolakis, 1988: *Introduction to Digital Signal Processing*. Macmillan Publishing Co., 944 pp.

Ryzhkov, A. V., and D. S. Zrnić, 1995: Comparison of dual-polarization radar estimators of rain. *J. Atmos. Oceanic Technol.*, **12**, 249–256.

Ryzhkov, A. V., and D. S. Zrnić, 1996: Assessment of rainfall measurement that uses specific differential phase. *J. Appl. Meteor.*, **35**, 2080–2090.

Ryzhkov, A. V., S. E. Giangrande, and T. J. Schuur, 2005: Rainfall estimation with a polarimetric prototype of the WSR-88D. *J. Appl. Meteor.*, **44**, 502–515.

Sachidananda, M., and D. S. Zrnic, 1987: Rain rate estimates from differential polarization measurements. *J. Atmos. Oceanic Technol.*, **4**, 588–598.

Scarchilli, G., E. Gorgucci, V. Chandrasekar, et al., 1993: Rainfall estimating using polarimetric technique at C-band frequencies. *J. Appl. Meteor.*, **32**, 1150–1160.

Schneebeli, M., and A. Berne, 2012: An extended Kalman filter framework for polarimetric X-band weather radar data processing. *J. Atmos. Oceanic Technol.*, **29**, 711–730.

Ulbrich, C. W., 1983: Natural variations in the analytical form of the raindrop size distribution. *J. Appl. Meteor.*, **22**, 1764–1775.

Vulpiani, G., M. Montopoli, L. D. Passeri, et al., 2012: On the use of dual-polarized C-band radar for operational rainfall retrieval in mountainous areas. *J. Appl. Meteor. Climatol.*, **51**, 405–425.

Wang, Y., and V. Chandrasekar, 2009: Algorithm for estimation of the specific differential phase. *J. Atmos. Oceanic Technol.*, **26**, 2565–2578.

Wilson, J. W., and E. A. Brandes, 1979: Radar measurement of rainfall—A summary. *Bull. Amer. Meteor. Soc.*, **60**, 1048–1058.

Zrnic, D., and A. Ryzhkov, 1996: Advantages of rain measurements using specific differential phase. *J. Atmos. Oceanic Technol.*, **13**, 454–464.